

A systematic first-principles study of surface energies, surface relaxation and Friedel oscillation of magnesium surfaces

Jia-Jun Tang^{1,2,3}, Xiao-Bao Yang^{1,2}, LiuZhang OuYang^{2,3}, Min Zhu^{2,3} and Yu-Jun Zhao^{1,2}

¹ Department of Physics, South China University of Technology, Guangzhou 510640, People's Republic of China

² Key Laboratory of Clean Energy Materials of Guangdong Higher Education Institute, South China University of Technology, Guangzhou 510640, People's Republic of China

³ School of Materials Science and Engineering, South China University of Technology, Guangzhou 510640, People's Republic of China

E-mail: zhaoyj@scut.edu.cn

Received 24 September 2013, revised 7 January 2014

Accepted for publication 23 January 2014

Published 26 February 2014

Abstract

We systematically study the surface energies and surface relaxations of various low-index and high-index Mg surfaces. It is found that low-index surfaces are not necessarily stable as Mg(1 0 $\bar{1}$ 0) is the most unstable surface in the series of Mg(1 0 $\bar{1}$ n) ($n = 0-9$). A surface-energy predicting model based on the bond cutting is proposed to explain the relative surface stabilities. The local relaxations of the low-index surfaces could be explained by the Friedel oscillation. For the high-index surfaces, the combination of charge smoothing effect and dramatic charge depletion influences the relaxations, which show a big difference from the low-index ones. Our findings provide theoretical data for considerable insights into the surface energies of hexagonal close-packed metals.

Keywords: surface energy, surface relaxation, friedel oscillation, Mg surfaces, high index, charge smoothing, hcp

(Some figures may appear in colour only in the online journal)

1. Introduction

Magnesium (and its alloys) has a broad application with its excellent physical and mechanical properties. For instance, it is widely used in automotive and aerospace industry due to its high strength/weight ratio [1]. It is also an intensively studied hydrogen storage material due to its high gravimetric hydrogen content, high volumetric density [2] and the highest energy density [3], i.e. 9 MJ kg^{-1} Mg. Thus, the hydrogen sorption properties of Mg and MgH_2 have been paid wide attention [4, 5] in recent years.

Mg surface properties including surface energies and structures are of considerable importance to hydrogen sorption. Surprisingly, the systematic study of surface energy and surface relaxation of Mg is still not available. Surface energy that describes the energy cost required for creation of surface

is a determinant of surface stability. Metal surfaces often experience surface relaxation, which lowers the surface free energy by small and subtle rearrangement of the surface atoms. A systematic study of the Mg surface is required for deeper insight into Mg surface stabilities. Theoretically, the Mg surface-energy metal could be described by the bond breaking model, which has been adopted to noble metals [6]. With technical tools including GGA [7–10] functionals [11–14] and data-analysing methods [15–17], it is possible for the accurate theoretical investigation of surface properties of magnesium metal. Recent literature [18–21] has studied some particular properties of the Mg(0001) surface, but without mention of Mg surface stabilities. Efforts [22–23] have been made to calculate the surface energies of hexagonal Mg but they merely focused on the (0001) surface. Meanwhile, high-index Mg surfaces may be involved in the

well-reported promotion of hydrogenation/dehydrogenation properties of Mg–H systems via the ball milling treatment [24]. Unfortunately, knowledge of the Mg surface is lacking and not enough to provide more insights into these experimental phenomena. Meanwhile, some previous papers [25–27] showed that the Friedel oscillation [28, 29] performed well on low-index Mg surfaces and was able to describe the Mg surface relaxation. Nevertheless, the feasibility of Friedel oscillation [28, 29] on the high-index surface relaxation is not clear.

It is intriguing to see how the basal and non-basal bonds (see figure 1) affect the surface energy. It is well known that the basal plane [30], the close-packed plane perpendicular to the principle axis, i.e. the c -axis, of hexagonal close-packed (hcp) Mg has higher thermodynamic stability due to its higher in-plane bond density. Sandloebes *et al* [31] have observed the Mg non-basal plane deformation, rather than the basal one. Therefore, the distinction between basal and non-basal bonds should be interesting. Moreover, Finnis *et al* [32] proposed a charge smoothing effect that also impacts the atom relaxation of surface. Thus, the combination effect of Friedel oscillation and charge smoothing effect of surface relaxation should be prudently considered.

In this paper, we have systematically studied the surface energies and local structures of various low- and high-index Mg surfaces. A mathematical model, based on concepts of basal and non-basal bonds, is set up for evaluating the surface energies. The mechanisms that influence the surface relaxations, including the Friedel oscillation and the charge smoothing effect, are used to describe the local structure of low- and high-index Mg surfaces. The methodologies are detailed in section 2, the results are given and discussed in section 3, and the conclusions are in section 4.

2. Methodologies

2.1. Computational details

The electron self-consistent calculations are conducted using the Vienna Ab-initio Simulation Package (VASP) [33, 34] with the framework of a plane-wave basis set and the projector augmented wave (PAW) [35, 36]. The Perdew, Burke and Ernzerhof (PBE) [7] and Perdew–Wang (PW91) [9, 14] functionals are used as the exchange-correlation potential. Mg:2p⁶3s² are treated as the valence electrons in the PAW pseudopotentials. In the calculations of all the surfaces considered, both the unrelaxed and relaxed situations are included with k -point meshes that show excellent converged results. The energy cutoff is set to be 310 eV. For the structural relaxation, a force criterion of 0.02 eV Å⁻¹ is adopted. Table 1 lists the numbers of layers of various calculated Mg surfaces. For each surface, a 1×1 cell is built with a vacuum of over 15 Å.

2.2. Convergence of surface-energy calculations

Surface energy is defined as the energy cost of creating the surface by dividing a crystal into two parts. There are three factors [37] that influence the surface energy of a

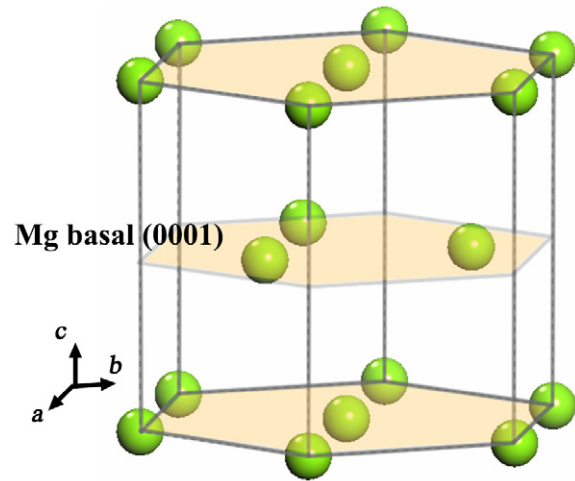


Figure 1. Schematic diagram of Mg basal planes and bonds. The basal (0001) is the close-packed plane vertical to the principle c -axis. Three Mg basal (0001) planes are indicated transparently. The bonds inside and outside the basal planes are basal and non-basal bonds, respectively.

specific surface: (i) the cutting bonds required; (ii) the surface reconstruction (surface atom relaxation); (iii) the contribution of vibrational entropy [38] and formations [39] of step and kink. The contribution of vibrational entropy would be negligible at low temperature, and it is not considered for the surface stability in this work. In our calculations, the contributions of the cutting bonds with and without surface reconstruction (it depends on whether the relaxation of atoms is allowed in the calculation) are considered. The procedure to calculate the surface energy is to evaluate the difference between the total energy $E^{\text{tot}}(n)$ of a slab with n atoms and the bulk energy E_{bulk} with the same number of atoms. The formula is as follows:

$$E_{\text{surf}} = \lim_{n \rightarrow \infty} \left(\frac{1}{2A} (E^{\text{tot}}(n) - E_{\text{bulk}}(n)) \right), \quad (1)$$

where A is the area of the surface slab and the factor 2 denotes that two surfaces are created in a slab model.

It has been an interesting story for the data analysis of surface energy. According to previous works [15–17], this procedure may encounter an unexpected problem of non-convergence caused by the unavoidable discrepancies between the two bulk energies calculated in the bulk-form model and the slab-form model, respectively. The reason is found [15] to be the sensitive dependence of slab total energy on the choice of different basis or k -point grids. Thus solutions [15–17] were proposed, one of which was the so-called Boettger method [15], which argued that the value E_{bulk} should be replaced by the incremental energy calculated by the subtraction between two slabs with atom numbers of n and $n - 1$. The *slab approach* [16], namely the Fiorentini method, whose idea is to improve the Boettger method [15] and where the value E_{bulk} is extracted by fitting the slab data, has been proven to improve the convergence efficiently [17]. Recently, another convergence method for surface-energy data analysis was proposed [17], so-called *direct method*, which requires that

Table 1. Numbers of layers of various calculated Mg surfaces. For each Miller index surface, we calculated six slabs with incremental thickness (0.5 or 1 layer). Here, one Mg layer consists of two Mg atoms. Thus, half a layer corresponds to one atom. Various layer thicknesses are considered. All of these thicknesses are thick enough to show convergence of surface energies, which are manifested to be very quantitatively close.

Surface index	0001	10 $\bar{1}$ 0	10 $\bar{1}$ 1	10 $\bar{1}$ 2	10 $\bar{1}$ 3	10 $\bar{1}$ 4	10 $\bar{1}$ 5
Number of layers	12.5–15	12–17	12–17	12.5–15	12.5–15	12.5–15	13.5–16
Surface index	10 $\bar{1}$ 6	10 $\bar{1}$ 7	10 $\bar{1}$ 8	10 $\bar{1}$ 9	11 $\bar{2}$ 0	21 $\bar{3}$ 0	
Number of layers	14.5–17	15.5–18	16.5–19	17.5–20	11–16	13–18	

the k -mesh is large enough to be accurate to yield the E_{bulk} within the independent bulk calculation. This is very close to the one extracted by the slab data to draw similar results. Comparing all the three methods mentioned above in the test calculations, we decided to adopt mainly the *slab approach* due to its relatively high efficiency in our calculations of pure magnesium.

The exchange-correlation functional that provides an accurate description of slowly varying electron densities [40] is required for accurate surface calculations. PBEsol [13], a new exchange-correlation functional, that recovers the gradient expansion for exchange over a wide range of electron density is constructed to yield excellent surface exchange energies, which are dominated by moderate density gradients. Ropo *et al* [41] have proved that PBEsol provided satisfactory surface results for various metallic bulk and surface systems. Thus, we adopt PBEsol in addition to using the conventional PBE and PW91 functionals.

2.3. Friedel oscillation

The surface relaxation, due mainly to the atomic charge deficiency in the beyond-surface region, can be largely described by the distribution of charge densities [32]. The model of smoothing of the charge density, proposed by Finnis *et al* [32], based on the Smolouchowski's [42] concept was adopted to describe the phenomenon of the atom relaxation. Moreover, a rational explanation was given by the Pauling chemical model [43] based on the bond-energy–bond-order relation. However, though the explanations seemed to be good on some systems, more persuasive explanations [25–27, 44–45] on surface relaxations were provided by the Friedel oscillation [28, 29]. On the jellium model, the well-known form [29, 45] of the Friedel oscillation is given by $\Delta\rho(z)/\rho_0 \sim 1/(2k_F z)^2 \cos(2k_F z + \phi)$, where ρ_0 is the mean electron density in the bulk, k_F is the bulk Fermi wave vector for a free electron gas, z is the distance from the surface and ϕ is a phase factor.

The Friedel oscillation method is used to describe the surface relaxation of our models. Noticeably, there are some previous Friedel oscillation studies [25, 26] on Mg surfaces with the local-density approximation (LDA) [46] functional. Based on the good description of surface of the sound PBEsol, the surface Friedel oscillation and its influence on the surface reconstruction are expected to be well described. Comparisons between our results and previous LDA ones will be made.

Table 2. Comparisons between the calculated Mg lattice parameters and those obtained with available data.

Method	a (Å)	c/a ratio	References
PW91	3.186	1.632	This study
PBE	3.192	1.635	This study
PBEsol	3.171	1.633	This study
PW91	3.21	1.62	[20]
RPBE, PBE	3.19	1.62	[47, 19]
FLAPW	3.21	1.62	[48]
Experiment	3.2093	1.623	[49]
Experiment	3.2094	1.623	[50]
Experiment	3.2344	1.624	[51]

3. Results and discussions

3.1. Bulk calculations

The Mg bulk is calculated with the PW91, PBE and PBEsol functionals, as the lattice and internal coordinates are fully relaxed. The calculated lattice constant a and the ratio of c/a are listed in table 2, along with experimental and theoretical values from the literature. The calculated values from all the three functionals show good agreement with the previous theoretical and experimental results. As listed in table 2, the results from the PBEsol functional are as reasonable as the other two.

3.2. Surface energy

Figure 2 shows the results of various Mg surface energies analysed using the *slab approach* [16] that are calculated with the three functionals (PW91, PBE and PBEsol). Thirteen surfaces including the low-index and high-index ones are included. It could be found that all the surface energies are in good convergence, and the relative stabilities are consistent by the three functionals. The relative stabilities of Mg surfaces are clearly shown in figure 2. For the unrelaxed surfaces, Mg(0001) is the most stable one while Mg(10 $\bar{1}$ 0), Mg(10 $\bar{1}$ 2), Mg(11 $\bar{1}$ 0) and Mg(21 $\bar{3}$ 0) show the highest surface energies. The surface energies of other surfaces are very close. Naturally, the interest of investigation of the relative stabilities arises.

Taking the PBEsol data as an example, we find that the Mg(0001) surface is the most stable as its surface energy is obviously lower than the others. In particular, the Mg(0001) surface energy is converged to be $39 \text{ meV } \text{Å}^{-2}$, which is nearly $7 \text{ meV } \text{Å}^{-2}$ lower than $46 \text{ meV } \text{Å}^{-2}$ of the second most stable Mg(10 $\bar{1}$ 1).

While the high stability of the Mg(0001) could be acceptable as it has the lowest index, the highest surface energy

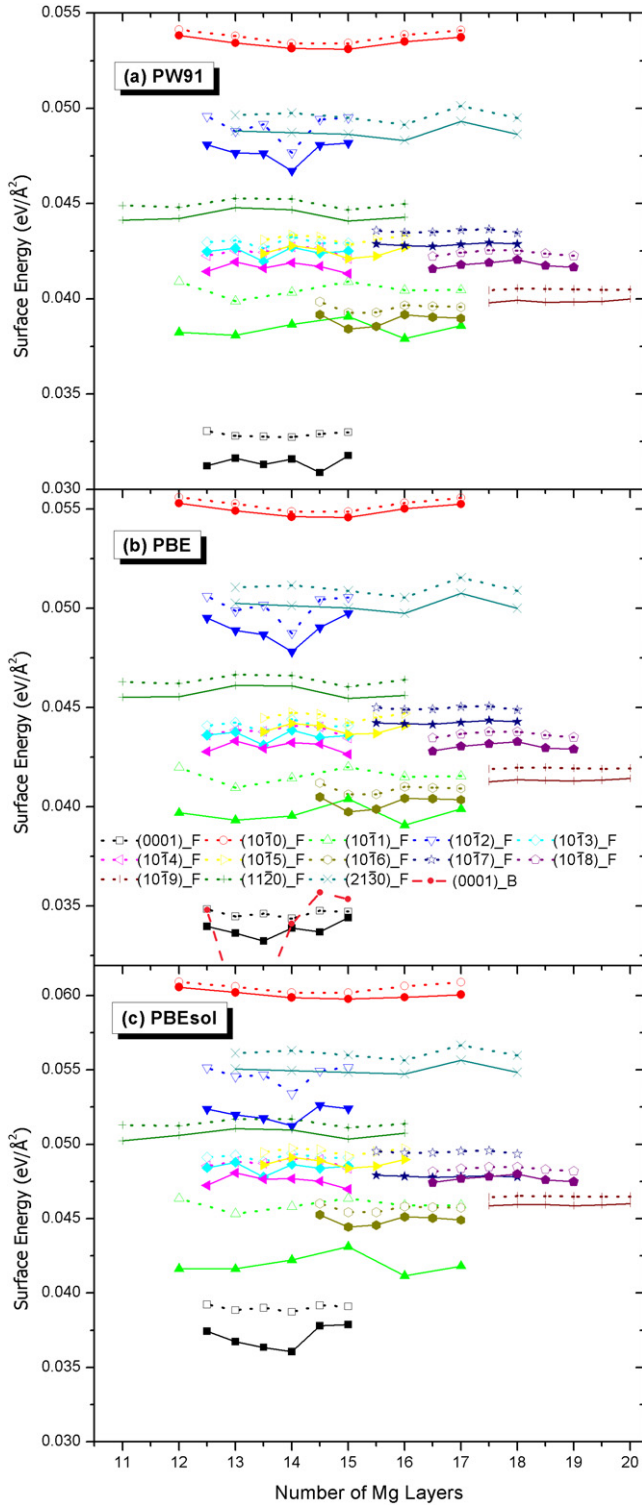


Figure 2. Magnesium surface energies calculated with the (a) PW91, (b) PBE and (c) PBEsol. The hollow and solid circles denote the unrelaxed and relaxed surfaces, respectively. One Mg layer consists of two Mg atoms. All the data are analysed using the *slab approach* [16] (denoted as ‘F’) except the data of (0001)_B that is analysed by the Boettger method [15] in (b).

of the Mg(10 $\bar{1}$ 0) surface seems to be puzzling although it is of low index. To rationalize the relative stabilities, we state that the contributions of cutting the basal bonds and the non-basal ones vary remarkably. More specifically, the bonds in

the hcp Mg are divided into two groups: the bonds within and outside the basal planes, namely the close-packed surfaces. Due to the slight differences between the bond lengths and the densities of these two kinds of bonds, it should be prudently supposed that the energies required to cut them also vary. The numbers of both the broken basal and non-basal bonds of the surfaces are listed in table 3 where the average numbers per unit square angstrom are also listed. It is assumed that the calculated surface energies (in $\text{meV } \text{\AA}^{-2}$) are the function of broken numbers of the basal and non-basal bonds. It could be found by solving the over-determined equations, namely by simple data fitting, that the energies needed to make the bond cuttings are $65.8 \text{ meV } \text{\AA}^{-2}$ and $59.4 \text{ meV } \text{\AA}^{-2}$, respectively. The two values differ by 10.77%, which is not negligible. It is, however, rational due to the relatively stronger bonding within the close-packed plane. As a result, a simple estimation for predicting the Mg surface energies could be written as

$$E_{\text{surf}} = n_{\text{basal}} \times E_{\text{basal}} + n_{\text{non-basal}} \times E_{\text{non-basal}}, \quad (2)$$

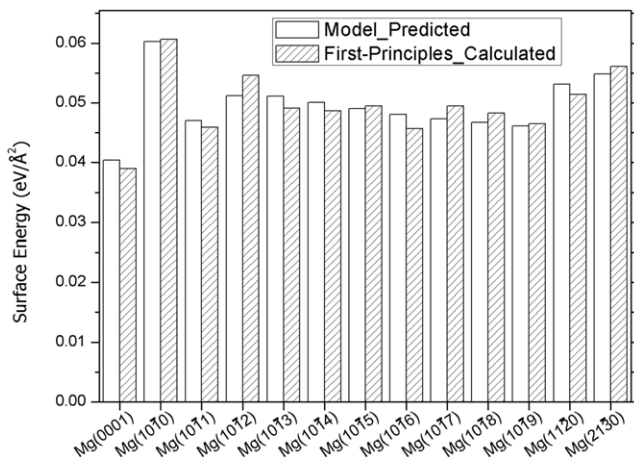
where n represents the number of cutting bonds and E_{basal} and $E_{\text{non-basal}}$ indicate the energies required for the basal and non-basal bond cuttings, namely $65.8 \text{ meV } \text{\AA}^{-2}$ and $59.4 \text{ meV } \text{\AA}^{-2}$, respectively. With this bond model, it could be known that the total number of bond cuttings and the percentages of basal and non-basal bonds contribute to surface stability. Following this simple logic, we conclude that the Mg(10 $\bar{1}$ 0), (10 $\bar{1}$ 1), (11 $\bar{2}$ 0) and (21 $\bar{3}$ 0) surfaces are the most unstable because their numbers of broken basal bonds are relatively large (being 0.482 \AA^{-2} , 0.426 \AA^{-2} , 0.556 \AA^{-2} and 0.546 \AA^{-2} , respectively, as listed in table 3). The comparisons between the model-predicted and the first-principles calculated results confirm this prediction (see table 3). The stability of Mg(10 $\bar{1}$ 1) is partly because of its relatively lower number of broken non-basal bonds while the instability of Mg(10 $\bar{1}$ 2) is partly due to its relatively high number of broken non-basal bonds. Overall, the deviations between the model-predicted and the first-principles calculated values are reasonable although the maximum absolute value is 6.19% (shown in figure 3). In addition to the errors from the bond model itself, the deviations may also be caused by the analysis error of the *slab approach* [16], and the error of the solutions of the over-determined equations, etc.

Briefly, it could be concluded that the Mg(0001) surface is the most stable due to no basal bond cuttings while the surfaces with major cutting of basal bonds are the most unstable ones. The contributions of the basal and non-basal bonds are found to vary. Therefore, the high-index hcp surfaces, such as Mg(10 $\bar{1}$ 5) and Mg(10 $\bar{1}$ 9), show higher stabilities than the low-index Mg(10 $\bar{1}$ 0). The high stability of the Mg(0001) surface is confirmed by a recent experiment [31] where the non-basal deformation, rather than the basal one, is observed.

It is also noticed that the PBEsol functional leads to higher surface energies, about $5 \text{ meV } \text{\AA}^{-2}$ for each surface, than the other two functionals. This is quite understandable due to the fact [13, 40, 52] that the PBEsol is less dependent on the density gradient, which causes the reduction of surface energies inevitably. It should also be pointed out that the Boettger method [15] for data analysis is also adopted (shown

Table 3. Statistics for the numbers of broken basal and non-basal bonds and the surface energies of Mg surfaces.

Surface Index	Area (\AA^{-2})	Number of basal/non-basal bonds (2 surfaces)	Number of basal bonds (\AA^{-2})/percentage of basal bonds (%)	Number of non-basal bonds (\AA^{-2})/percentage of non-basal bonds (%)	The model-predicted/first-principle calculated surface energies (meV \AA^{-2})	Deviation (%)
0001	8.81	0/6	0/0	0.681/100	40.4/39	3.71
10 $\bar{1}$ 0	16.62	8/8	0.482/50	0.482/50	60.3/60.6	-0.55
10 $\bar{1}$ 1	18.77	8/6	0.426/57.1	0.32/42.9	47/45.9	2.49
10 $\bar{1}$ 2	24.19	8/12	0.331/40	0.496/60	51.2/54.6	-6.19
1013	31.20	8/18	0.256/30.7	0.577/69.3	51.1/49.1	4.17
10 $\bar{1}$ 4	38.96	8/24	0.205/25	0.616/75	50.1/48.7	2.88
10 $\bar{1}$ 5	47.10	8/30	0.170/21	0.637/79	49/49.5	-0.98
10 $\bar{1}$ 6	55.38	8/36	0.144/18.1	0.650/81.9	48.1/45.7	5.28
10 $\bar{1}$ 7	63.93	8/42	0.125/16	0.657/84	47.3/49.5	-4.53
10 $\bar{1}$ 8	72.40	8/48	0.111/14.3	0.663/85.7	46.7/48.3	-3.41
10 $\bar{1}$ 9	81.08	8/54	0.099/12.9	0.666/87.1	46.1 / 46.5	-0.97
11 $\bar{2}$ 0	28.78	16/8	0.556/66.7	0.278/33.3	53.1/51.4	3.31
21 $\bar{3}$ 0	44.03	24/14	0.546/63.2	0.318/36.8	54.8/56.1	-2.38

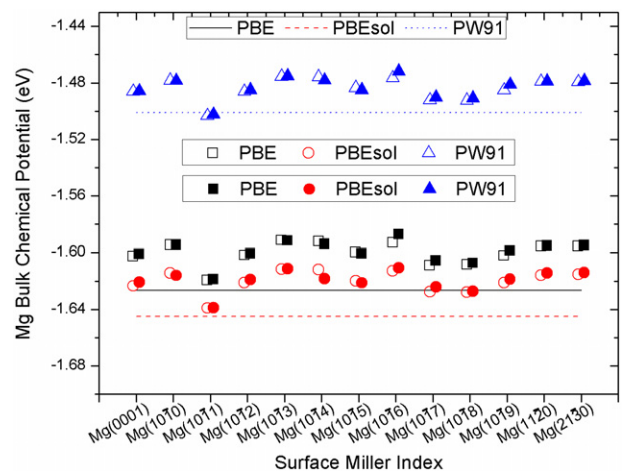
**Figure 3.** The comparison of model-predicted and first-principles calculated surface energies of various Mg surfaces.

in figure 2(b)). As is seen, the convergence of the Mg(0001) surface is not as satisfactory as the *slab approach* [16]. The differences, as shown in figure 4, between the calculated and the *slab-approach* [16] fitted bulk chemical potentials are always not negligible. In our data analysis of the unrelaxed and relaxed models, the fitted bulk chemical potential of the unrelaxed model (the hollow shapes in figure 4) is considered as the term $\mu_{\text{Mg,Bulk}}^{\text{fit}}$ in the surface-energy calculation for each surface.

After the discussion of the Mg unrelaxed surfaces, one may also be interested in the contribution of relaxation to the surface energies of Mg. Here, we arrange the discussion of the Mg surface relaxation to be in the next subsection, where systematic discussions on the relaxation will be performed from another point of view.

3.3. Surface relaxation

For a surface, the charge redistribution has a significant impact on the relaxation of surface atoms. The idea of Friedel oscillation [28], which is the analogue to electric charge screening of charged species in a pool of ions that is caused

**Figure 4.** The *slab-approach* [16] fitted Mg bulk chemical potentials. The neighbouring hollow and solid shapes denote the unrelaxed and relaxed models of the same Mg surface, respectively. Three horizontal lines represent the calculated Mg chemical potential in the bulk calculation.

by charge redistribution, is extended [29] to the electrostatic Coulomb attraction effect between the surface layers where the oscillation of charge depletion was observed. More specifically, Friedel oscillation causes charge accumulation or depletion in layer locality [26]. The ionic layers respond by moving closer or further apart depending on whether electrostatic force between them is attractive or repulsive. Then the relaxation of surface atoms could be well explained theoretically. Following the historical track, we adopt this method on the discussions of relaxations of Mg surface atoms. Noticeably, the surfaces on which we focus include not only the low-index ones but also the high-index ones, which were often neglected by previous works [26, 45]. Moreover, we also pay special attention to the charge smoothing effect which describes the charge transfer between the surface regions of low and high charge density due to the kinked contour of charge density [45].

The Friedel oscillation study of low and high-index Mg surfaces are exemplified by Mg(0001), Mg(10 $\bar{1}$ 0),

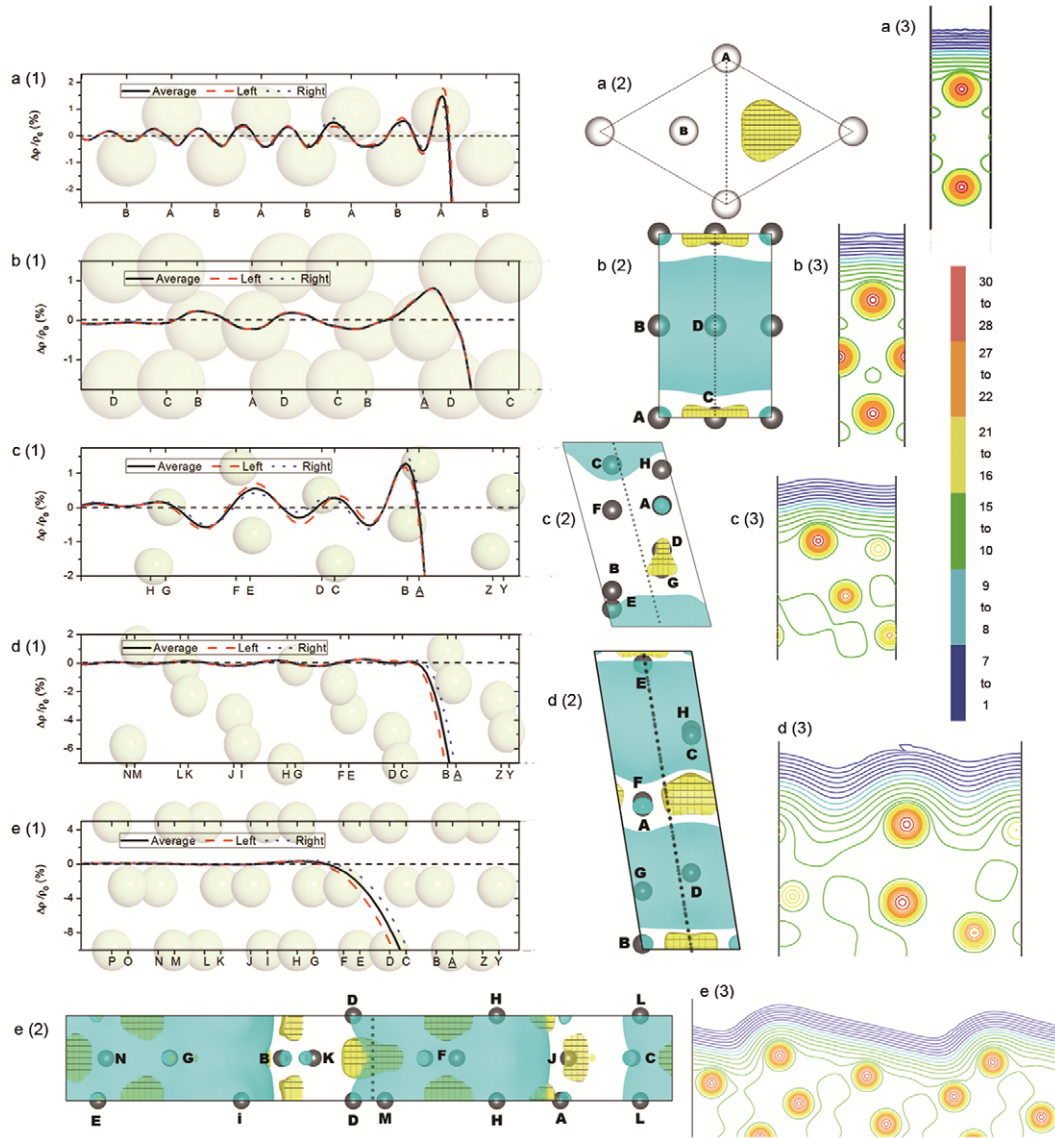


Figure 5. Friedel oscillation versus z : (a1) $\text{Mg}(0001)$, (b1) $\text{Mg}(10\bar{1}0)$, (c1) $\text{Mg}(10\bar{1}1)$, (d1) $\text{Mg}(10\bar{1}3)$ and (e1) $\text{Mg}(10\bar{1}8)$. Vertical view of charge transfer on (a2) $\text{Mg}(0001)$, (b2) $\text{Mg}(10\bar{1}0)$, (c2) $\text{Mg}(10\bar{1}1)$, (d2) $\text{Mg}(10\bar{1}3)$ and (e2) $\text{Mg}(10\bar{1}8)$. Cross section of charge densities of (a3) $\text{Mg}(0001)$, (b3) $\text{Mg}(10\bar{1}0)$, (c3) $\text{Mg}(10\bar{1}1)$, (d3) $\text{Mg}(10\bar{1}3)$ and (e3) $\text{Mg}(10\bar{1}8)$. The first surface layer is marked with the underline. The light blue and squared yellow colours in the charge transfer paragraphs (the (a2), (b2), (c2), (d2) and (e2) graphs) represent charge depletion and accumulation in the surface region. The colour bar indicates the extent of the charge densities. The number on the right-hand side of the bar denotes the ordinal number of the lines in the plots of charge densities (from low to high). The amount of charge density of a specific line could be calculated by the equation $\rho = 0.001 \times (\sqrt{2})^n$. The colour of the lines is a guide to the eye.

$\text{Mg}(10\bar{1}1)$, $\text{Mg}(10\bar{1}3)$ and $\text{Mg}(10\bar{1}8)$ surfaces. As shown in figure 5, we find that the Friedel oscillation performs well in the low-index surfaces, namely $\text{Mg}(0001)$, $\text{Mg}(10\bar{1}0)$ and $\text{Mg}(10\bar{1}1)$. Oscillatory variations of $\Delta\rho(z)/\rho_0$ could be clearly seen on these surfaces. The relaxations of layer could also be explained by the charge accumulation or depletion (discussed in the next two paragraphs). Comparatively, the Friedel oscillations do not perform well on the high-index surfaces $\text{Mg}(10\bar{1}3)$ and $\text{Mg}(10\bar{1}8)$, where a dramatic surface charge depletion happens (see figures 5(d) and (e)). There are two observations: (i) the areas of charge depletion take up nearly 75% of the unit cell and (ii) the distribution of the region of charge accumulation is separate in the space. They could be explained by two facts of these two high-index

surfaces: (i) less regular arrangement of surface atoms leads to kinked charge distribution (see figure 5); (ii) the small interlayer distances along the z direction that facilitate the charge transfer from the surface to the deep bulk region. As a result, dramatic charge depletion tends to dominate on the high-index surfaces. Moreover, the charge smoothing effect induced by the kinked contour of electric potential leads to separate charge accumulation. As shown in figures 5(d2) and (e2), the separate distribution of charge accumulation regions also explains the obvious distinctions of quantities of charge depletion between the left and right half cells.

Distinct from the high-index surfaces, the low-index ones have a relatively more regular arrangement of surface atoms resulting in a less kinked contour of charge density.

Table 4. Details of surface atom-specific relaxations or layer-specific information. The number i or j represents the i th or j th atom distanced from surface. The letter R denotes the interlayer region between the i th and j th layers. $\Delta\rho(z)/\rho_0$ means the same as the vertical axis of figure 5(a1). Δd_{ij} , shown in italics, indicates the variation of interlayer distances. D is the atomic displacement and Dz/D is the ratio of the displacement along the z direction to the total displacement after relaxation. For Mg(10 $\bar{1}$ 1), Mg(10 $\bar{1}$ 3) and Mg(10 $\bar{1}$ 8) surfaces, there are several interlayer distances not being calculated because they are very small.

Layer	Mg(0001)		Mg(10 $\bar{1}$ 0)		Mg(10 $\bar{1}$ 1)	
	$\Delta\rho(z)/\rho_0$ (\pm)	$D(\text{\AA})/Dz/D$ (%) or Δd_{ij} (%), shown in bold italics)	$\Delta\rho(z)/\rho_0$ (\pm)	$D(\text{\AA})/Dz/D$ (%) or Δd_{ij} (%)	$\Delta\rho(z)/\rho_0$ (\pm)	$D(\text{\AA})/Dz/D$ (%) or Δd_{ij} (%)
1	–	0.174/99.97	–	0.027/100	–	0.324/97.96
R _{1,2}	+	–1.61	0	–1.37		
2	–	0.133 / 99.76	+	0.002/100		0.258/99.81
R _{2,3}	+	–0.79	+	–2.67	+	–3.58
3	–	0.112/99.97	+	0.027/100	–	0.178/99.43
R _{3,4}	0	–2.37	0	–2.8		
4	+	0.052/98.17	–	0.025/100		0.225/99.01
R _{4,5}	–	–1.69	0	0.74	+	–3.31
5	+	0.008/85.51	+	0.018/100	–	0.117/90.07
R _{5,6}	–	–0.81	0	0.72		
6	+	0.015/91.69	–	0.005/100		0.138/96.15

Layer	Mg(10 $\bar{1}$ 3)		Mg(10 $\bar{1}$ 8)	
	$\Delta\rho(z)/\rho_0$ (\pm)	$D(\text{\AA})/Dz/D$ (%) or Δd_{ij} (%)	$\Delta\rho(z)/\rho_0$ (\pm)	$D(\text{\AA})/Dz/D$ (%) or Δd_{ij} (%)
1	–	0.049/98.64	+	0.237/83.30
2		0.057/90.99		0.125/90.71
R _{12,34}	+	–4.87	+	–12.12
3	–	0.046/99.00	+	0.043/67.53
4		0.049/94.96		0.031/97.38
R _{34,56}	+	1.68	+	–6.94
5	–	0.031/26.85	+	0.031/94.74
6		0.015/87.87		0.031/92.24

Thus less charge smoothing effect is observed on these surfaces, especially for the Mg(10 $\bar{1}$ 0), where the unit cell is in mirror symmetry along the dashed plane (vertical to the paper) in figure 5(c2) and therefore the contour of charge density is also in mirror symmetry (see figure 5(b3)) and no charge smoothing effect happens. On the Mg(0001) and Mg(10 $\bar{1}$ 1) surfaces, the slight charge smoothing effect could still be observed. As mentioned earlier, this is caused by the asymmetric arrangement, which dovetails with the kinked contour of the charge densities, of atoms in the left and right half cells. Consequently, the quantities of the charge transfer, as shown in figures 5(a1) and (c1) of the left and right half cells, are slightly distinct. Moreover, the charge tends to accumulate in the regions with lower atomic densities.

The discussions of the previous few paragraphs detail the factors that influence the charge redistribution when a surface is created. To probe more deeply into the relaxation of Mg surface atoms, a summarization of the charge distribution and atomic displacement of five surfaces is listed in table 4. We find that the variations of interlayer distances agree well with the analysis of Friedel oscillation on the low-index surfaces. For instance, the charge tends to accumulate on the first, second and third layers on Mg(0001), while the interlayer regions between them witness the charge depletion. This phenomenon gives a series of sign of ‘– + – + –’ which represent the charge accumulation (– net charge becomes more negative) and depletion (+ net charge becomes more positive). Thus the Coulomb attraction between the first layer and the

neighbouring interlayer region takes place. The same happens to the second layer so that the d_{12} contracts and the variation of d_{12} is -1.61% . According to table 4, it could be concluded that this simple Friedel analysis could well explain the relaxations of atoms on the low-index surfaces. It could also be found that the relaxation of surface atoms, on the low-index surfaces, is mainly towards the bulk perpendicularly, especially for the Mg(10 $\bar{1}$ 0) where the ratio Dz/D reaches 100%, which means the in-plane relaxation is negligible. However, the Friedel oscillation is much less obvious on the high-index Mg(10 $\bar{1}$ 3) and Mg(10 $\bar{1}$ 8), where the charge depletion and the charge smoothing effect dominates. The dramatic charge depletion always dovetails with the remarkable contractions of interlayer distances. Taking the Mg(10 $\bar{1}$ 8) as the example, the contractions of d_{12} , d_{23} and d_{34} are up to -12.12% , -6.94% and -6.82% . We also observe that the interlayer Coulomb effect and the charge smoothing effect impact the system together. The values of surface atom-specific ratio Dz/D reflect that the dramatic charge depletion has a remarkable impact on notable contractions of interlayer distances. More specifically, both the xy -plane displacement caused mainly by the charge smoothing effect and the z direction relaxation induced mainly by dramatic charge depletion happen to the surface atoms.

The surface energies are lowered after surface relaxation. As shown in figure 2(c), the reduction in surface energy ranges from about 0.5 meV \AA^{-2} (Mg(10 $\bar{1}$ 0)) to 2 meV \AA^{-2} (Mg(10 $\bar{1}$ 1)). It is interesting to find that

Mg(10 $\bar{1}$ 1) exhibits the greatest reduction in surface energy after surface relaxation among the Mg(10 $\bar{1}$ n) surfaces (n is from 1 to 9). Moreover, a seeming trend that the reduction gets smaller as n increases could be also observed. From the view point of the bond cutting model mentioned earlier, it is understandable because the Mg(10 $\bar{1}$ 1) has the most basal bonds and the least non-basal bonds cut. Basal bonds that have more bond energy imply stronger binding to the surface atoms. Thus more cuttings correspond to less binding to the surface atoms and it leads to a greater displacement of relaxation (see table 4) which could be reflected by a greater reduction in surface energy after relaxation. The atomic displacements on Mg(10 $\bar{1}$ 1) are all larger than those of Mg(10 $\bar{1}$ 3) and Mg(10 $\bar{1}$ 8) although the two Mg(10 $\bar{1}$ 8) outermost atoms experience a long displacement. The difference of number of broken bonds explains the reduction in the relaxed surface energies. One may feel curious about the small reduction of relaxed Mg(10 $\bar{1}$ 0) surface energy. It is, *ipso facto*, attributed to the high symmetry of this surface that dovetails with the symmetric charge distribution and small variation of charge transfer (see figure 5(b1)).

To show the dependence of charge distribution on the structure symmetry, we also plot the contour graphs of charge densities on the surfaces. It could be seen that the low-index surfaces have more flat contours while the contours of the high-index surfaces are more kinked. Even a huge fluctuation could be seen in the case of Mg(10 $\bar{1}$ 8).

Previous papers [25, 26] have also performed some calculations on the Mg(0001) and (10 $\bar{1}$ 0) surface relaxations with LDA functionals. Comparatively, our results of Mg(0001) and Mg(10 $\bar{1}$ 0) surface show a less abrupt change of the amount of charge variation in the surface region. For example, the percentage of charge accumulation on the first Mg(0001) layer is nearly 2%, compared with 5% of [23]. The quantitative difference persists on the other Mg(0001) layers and leads to a different result of variations of interlayer distance. Namely, slight contractions of interlayer distance are observed in our calculation instead of the slight expansion found in [23]. Moreover, our results of Mg(10 $\bar{1}$ 0) show consistency with those of previous LDA results [25, 26]. The distinction between our PBEsol result and the LDA one originates from a different accuracy of the description of surface exchange energy. The difference between the basal and non-basal bond may be enlarged in the LDA calculation, and thus the charge variation of surface layers is more obvious. With more accurate PBEsol, the charge variation could be more accurately described.

In brief, the Mg surface relaxation is found to be deeply influenced by the surface symmetry and the numbers of broken bonds.

4. Conclusions

In summary, we have systematically studied the surface energies and relaxations of various Mg surfaces. It is found that the surface energy of hcp Mg could be modelled by multiplying the energy required for cutting a bond and the number of broken bonds, as expected. Nevertheless, the bonds in or out of a

close-packed plane should be treated differently. Due to the differences between numbers of two kinds of broken bonds, the surface energies of various surfaces vary. The Friedel oscillation plays a vital role on the relaxations of low-index Mg surfaces while the relaxations of high-index Mg surfaces atoms are influenced by both the charge depletion and the charge smoothing effect. Our results provide considerable insight into the stabilities of Mg metal surface and may serve as a guide for the investigation of other metal surfaces.

Acknowledgments

This work was supported by MOST under project 2010CB631302, NSFC (Grant 11174082, 11104080), the Fundamental Research Funds for the Central Universities (Grant 2011ZM0090), and Guangdong Natural Science Foundation (S2011040005430). The computing resources from ScGrid of the Supercomputing Center, Computer Network Information Center of CAS, are gratefully acknowledged.

References

- [1] Gray J E and Luan B 2002 *J. Alloys Compounds* **336** 88–113
- [2] Selvam P, Viswanathan B, Swamy C S and Sprinivasan V 1986 *Int. J. Hydrog. Energy* **11** 169–92
- [3] Fukai Y 2005 *The Metal–Hydrogen System: Basic Bulk Properties* 2nd edn (Berlin: Springer) p 497
- [4] Jain I P, Lal C and Jain A 2010 *Int. J. Hydrog. Energy* **35** 5133–44
- [5] Zhu M, Lu Y, Ouyang L and Wang H 2013 *Materials* **6** 4654–74
- [6] Galanakis I, Bihlmayer G, Bellini V, Papanikolaou N, Zeller R, Blugel S and Dederichs P H 2002 *Europhys. Lett.* **58** 751–7
- [7] Perdew J P, Burke K and Ernzerhof M 1996 *Phys. Rev. Lett.* **77** 3865–8
- [8] Perdew J P, Burke K and Wang Y 1996 *Phys. Rev. B* **54** 16533–9
- [9] Perdew J P, Chevary J A, Vosko S H, Jackson K A, Pederson M R, Singh D J and Fiolhais C 1992 *Phys. Rev. B* **46** 6671–87
- [10] Perdew J P and Yue W 1986 *Phys. Rev. B* **33** 8800–2
- [11] Armiento R and Mattsson A E 2005 *Phys. Rev. B* **72** 085108
- [12] Perdew J P, Ernzerhof M and Burke K 1996 *J. Chem. Phys.* **105** 9982–5
- [13] Perdew J P, Ruzsinszky A, Csonka G I, Vydrov O A, Scuseria G E, Constantin L A, Zhou X and Burke K 2008 *Phys. Rev. Lett.* **100** 136406
- [14] Wang Y and Perdew J P 1991 *Phys. Rev. B* **43** 8911–6
- [15] Boettger J C 1994 *Phys. Rev. B* **49** 16798–800
- [16] Fiorentini V and Methfessel M 1998 *J. Phys.: Condens. Matter* **10** 895
- [17] Singh-Miller N E and Marzari N 2009 *Phys. Rev. B* **80** 235407
- [18] Chen M, Yang X B, Cui J, Tang J J, Gan L Y, Zhu M and Zhao Y J 2012 *Int. J. Hydrog. Energy* **37** 309–17
- [19] Du A J, Smith S C, Yao X D and Lu G Q 2005 *J. Phys. Chem. B* **109** 18037–41
- [20] Jiang T, Sun L-X and Li W-X 2010 *Phys. Rev. B* **81** 035416
- [21] Tang J-J, Yang X-B, Chen M, Zhu M and Zhao Y-J 2012 *J. Phys. Chem. C* **116** 14943–9
- [22] Skriver H L and Rosengaard N M 1992 *Phys. Rev. B* **46** 7157–68
- [23] Wachowicz E and Kiejna A 2001 *J. Phys.: Condens. Matter* **13** 10767–76

- [24] Sadhasivam T, Sterlin Leo Hudson M, Pandey S K, Bhatnagar A, Singh M K, Gurunathan K and Srivastava O N 2013 *Int. J. Hydrog. Energy* **38** 7353–62
- [25] Cho J-H, Ismail, Zhang Z and Plummer E W 1999 *Phys. Rev. B* **59** 1677–80
- [26] Staikov P and Rahman T S 1999 *Phys. Rev. B* **60** 15613–6
- [27] Tang S J, Jeng H T, Ismail, Sprunger P T and Plummer E W 2009 *Phys. Rev. B* **80** 085419
- [28] Friedel J 1958 *IL Nuovo Ciemento Series X* vol 7 pp 287–311
- [29] Lang N D and Kohn W 1970 *Phys. Rev. B* **1** 4555–68
- [30] Kittel C 2005 *Introduction to Solid State Physics* 8th edn (Hoboken, NJ: Wiley) p 16
- [31] Sandloebes S, Zaefferer S, Schestakow I, Yi S and Gonzalez-Martinez R 2011 *Acta Mater.* **59** 429–39
- [32] Finnis M W and Heine V 1974 *J. Phys. F: Met. Phys.* **4** L37–41
- [33] Kresse G and Furthmüller J 1996 *Phys. Rev. B* **54** 11169–86
- [34] Kresse G and Furthmüller J 1996 *Comput. Mater. Sci.* **6** 15–50
- [35] Blöchl P E 1994 *Phys. Rev. B* **50** 17953–79
- [36] Kresse G and Joubert D 1999 *Phys. Rev. B* **59** 1758–75
- [37] Yu D K, Bonzel H P and Scheffler M 2006 *New J. Phys.* **8** 65
- [38] Frenken J W M and Stoltze P 1999 *Phys. Rev. Lett.* **82** 3500–3
- [39] Feibelman P J 1999 *Phys. Rev. B* **60** 11118–22
- [40] Perdew J P, Constantin L A, Sagvolden E and Burke K 2006 *Phys. Rev. Lett.* **97** 223002
- [41] Ropo M, Kokko K and Vitos L 2008 *Phys. Rev. B* **77** 195445
- [42] Smoluchowski R 1941 *Phys. Rev.* **60** 661–74
- [43] Pauling L 1931 *J. Am. Chem. Soc.* **53** 1367–400
- [44] Mans A, Dil J H, Ettema A R H F and Weitering H H 2005 *Phys. Rev. B* **72** 155442
- [45] Sun Y Y, Huan A C H, Feng Y P and Wee A T S 2005 *Phys. Rev. B* **72** 153404
- [46] Kohn W and Sham L J 1965 *Phys. Rev.* **140** A1133–8
- [47] Vegge T 2004 *Phys. Rev. B* **70** 035412
- [48] Da Silva J L F, Stampfl C and Scheffler M 2006 *Surf. Sci.* **600** 703–15
- [49] Straumanis M 1949 *J. Appl. Phys.* **20** 726–34
- [50] Walker C and Marezio M 1959 *Acta Metall.* **7** 769–73
- [51] Schimmel H G, Huot J, Chapon L C, Tichelaar F D and Mulder F M 2005 *J. Am. Chem. Soc.* **127** 14348–54
- [52] Sun J, Marsman M, Ruzsinszky A, Kresse G and Perdew J P 2011 *Phys. Rev. B* **83** 121410